# Distinct roles for GABA across multiple timescales in mammalian circadian timekeeping

Daniel DeWoskin[a], Jihwan Myung[b], Mino D. C. Belle[c], Hugh D. Piggins[c], Toru Takumi[b], and Daniel B. Forger[a,d,1]

[a]Department of Mathematics, University of Michigan, Ann Arbor, MI 48109; [b]RIKEN Brain Science Institute, Wako, Saitama 351-0198, Japan; [c]Faculty of Life Sciences, University of Manchester, Manchester M13 9PT, United Kingdom; and [d]Department of Computational Medicine and Bioinformatics, University of Michigan, Ann Arbor, MI 48109

Edited by Joseph S. Takahashi, Howard Hughes Medical Institute, University of Texas Southwestern Medical Center, Dallas, TX, and approved April 14, 2015 (received for review October 29, 2014)

**The suprachiasmatic nuclei (SCN), the central circadian pacemakers in mammals, comprise a multiscale neuronal system that times daily events. We use recent advances in graphics processing unit computing to generate a multiscale model for the SCN that resolves cellular electrical activity down to the timescale of individual action potentials and the intracellular molecular events that generate circadian rhythms. We use the model to study the role of the neurotransmitter GABA in synchronizing circadian rhythms among individual SCN neurons, a topic of much debate in the circadian community. The model predicts that GABA signaling has two components: phasic (fast) and tonic (slow). Phasic GABA postsynaptic currents are released after action potentials, and can both increase or decrease firing rate, depending on their timing in the interspike interval, a modeling hypothesis we experimentally validate; this allows flexibility in the timing of circadian output signals. Phasic GABA, however, does not significantly affect molecular timekeeping. The tonic GABA signal is released when cells become very excited and depolarized; it changes the excitability of neurons in the network, can shift molecular rhythms, and affects SCN synchrony. We measure which neurons are excited or inhibited by GABA across the day and find GABA-excited neurons are synchronized by—and GABA-inhibited neurons repelled from—this tonic GABA signal, which modulates the synchrony in the SCN provided by other signaling molecules. Our mathematical model also provides an important tool for circadian research, and a model computational system for the many multiscale projects currently studying brain function.**

GABA | circadian | mathematical modeling | synchronization | network

Animals time daily events with endogenously generated ~24-h (circadian) rhythms. Although circadian rhythms are generated intracellularly through transcription-translation feedback loops, organism-level timekeeping in mammals is coordinated by a neuronal network of around 20,000 neurons located in the suprachiasmatic nuclei (SCN) of the anterior hypothalamus. Among the many neurochemicals of importance for synchronization of tissue-level rhythms and intercellular signaling in the SCN (1, 2), γ-aminobutyric acid (GABA) is the only neurotransmitter that is produced and received by all or nearly all SCN neurons (3, 4). Nevertheless, the role of GABA in the SCN is still not well understood. Although GABA-elicited postsynaptic currents (PSCs) are generally hyperpolarizing (inhibitory) in most parts of the brain, in the SCN they can also be depolarizing (excitatory) (5–11), with a receiving cell's response to GABA dependent on its intracellular chloride concentration (11). The fraction and location of the GABA-excited SCN neurons is still debated. GABA is able to synchronize SCN rhythms (4) and is necessary for the synchronization of SCN subregions after disruption by light (12), phase shifts of the light/dark cycle (8, 13), or the compromising of molecular rhythms (14). Other studies have found, however, that GABA actively opposes synchrony by injecting jitter into rhythms (6), and that blocking GABA receptors increases synchrony in SCN slices (15), and peak firing rates, rhythm amplitude, and precision of cultured SCN neurons (16). Thus, the work of well-respected laboratories seems to produce opposite results on whether the primary signal in the SCN acts to synchronize, desynchronize, inhibit, or excite SCN neurons.

To investigate the role of GABA in the SCN, we use an integrative approach combining experiments and mathematical modeling. Despite numerous modeling studies (17–21), with some even describing GABA (22, 23), no model has yet been able to resolve the effects of GABA on their natural timescale of milliseconds in understanding circadian timekeeping. We use advances in computing on graphics processing units (GPUs) to simulate the billions of GABA PSCs that occur daily within the SCN. Our model builds on published and validated detailed molecular clock (24, 25) and electrophysiology models (26) to create a model of the SCN network that is able to resolve the molecular events generating intracellular rhythms and the electrical activities of each cell in the network down to individual action potentials. We show how this model, combined with novel physiological data, can resolve much of the controversy surrounding GABA in the SCN. Our work also shows the importance of detailed modeling of the brain, which has received much recent attention.

## Results

**Model Formulation.** In a previous study, we used a detailed model of the molecular clock in a single cell (24) as the basis for a multicellular SCN model with intercellular signaling through the neuropeptide vasoactive intestinal peptide (VIP) (25). Here, we

### Significance

**Each day, over 50 billion synaptic signals, mediated by the neurotransmitter GABA, are sent between neurons in the central circadian pacemaker in the mammalian brain to time and coordinate daily events. Although GABA is the only signaling molecule sent and received by most, if not all of these neurons, its role is not well understood. Past studies have shown paradoxically that GABA can synchronize and desynchronize, as well as excite and inhibit, clock neurons. Through experiments and modeling characterizing the role of GABA in timekeeping, we propose the existence of two types of differentially regulated GABA signaling—fast signaling that regulates neuronal output, and slow signaling that modulates synchrony between neurons—a hypothesis that can explain many previous experimental results.**

Author contributions: D.D., J.M., M.D.C.B., H.D.P., T.T., and D.B.F. designed research; D.D., J.M., and M.D.C.B. performed research; H.D.P., T.T., and D.B.F. contributed new reagents/analytic tools; D.D. and J.M. analyzed data; and D.D., H.D.P., T.T., and D.B.F. wrote the paper.

The authors declare no conflict of interest.

This article is a PNAS Direct Submission.

Freely available online through the PNAS open access option.

[1]To whom correspondence should be addressed. Email: forger@umich.edu.

This article contains supporting information online at www.pnas.org/lookup/suppl/doi:10.1073/pnas.1420753112/-/DCSupplemental.

greatly extend the multicellular model to make it multiscale by including each cell's electrophysiological activity, coupling between the molecular clock and electrical activity within each cell, and GABAergic signaling between the cells in the network. The connections between each of these components within a model cell are shown in Fig. 1, and are explained in detail in *Materials and Methods* and *SI Appendix*.

Briefly, molecular-clock phase (determined by E-box activity) controls two potassium channel conductances ($g_{KCa}$ and $g_{K-leak}$) leading to circadian variation in the resting membrane voltage and electrical activity of the cell. Membrane voltage can be further increased or decreased because of GABA signaling, with the polarity dependent on the GABA reversal potential ($E_{GABA}$) of the cell. Membrane voltage affects intracellular calcium concentrations, which can cause *Period 1* and *2* (*Per1* and *Per2*) transcription via activation of the cyclic AMP-response element (CRE) through phosphorylation of the CRE-binding protein (CREB). In simulations including VIP, VIP is assumed to be released only by ∼10% of the ventral SCN neurons. In these cells, VIP release is assumed to be dependent on intracellular calcium. VIP is assumed to diffuse quickly across the SCN and is received by all cells, because all cells express its receptor VIP receptor 2 (VPAC2) (27). After its release, VIP binds to extracellular VPAC2 receptors leading to CREB phosphorylation and subsequent *Per* transcription. Finally, the activity of the VPAC2 receptor is inhibited by cytosolic cryptochrome (CRY) protein (28). With these extensions, we are able to resolve all of the billions of action potentials and GABAergic PSCs in the SCN network in each simulated day, and study the effects of GABA signaling on SCN timekeeping. The details of the computational methods used to simulate the model on GPUs can be found in *SI Appendix*.

**Effect of GABA Signaling on SCN Neuron Electrical Activity.** We first use the model to predict the response of individual SCN neurons to GABA-induced PSCs. Our model makes an interesting prediction that goes against the prevailing thinking about the SCN (29, 30). In particular, we find that inhibitory PSCs given early in the interspike interval (ISI) can shorten the ISI and actually speed up firing. In contrast, inhibitory PSCs lengthen the ISI and slow down firing when presented at later phases during the ISI. Although the magnitude of this effect depends on the time of day, the trend is consistent throughout the daytime.

To test this prediction, we apply 10-pA hyperpolarizing (inhibitory) current pulses, 60 ms in duration (simulating ∼10 PSCs, a typical number seen during an ISI, presented simultaneously) to SCN neurons and measure the change in ISI caused by the pulses as described in *Materials and Methods*. Data for a sample neuron are shown in Fig. 2*A*. All data are grouped into 10 bins and plotted on top of the model predicted phase-response curve (PRC) in Fig. 2*B*. Our simulated PRC generated before the experiment match the data surprisingly well. In particular, we see that inhibitory pulses given shortly after an action potential shorten the length of the ISI, whereas pulses given later in the cycle tend to increase the length of the ISI, validating our hypothesis.

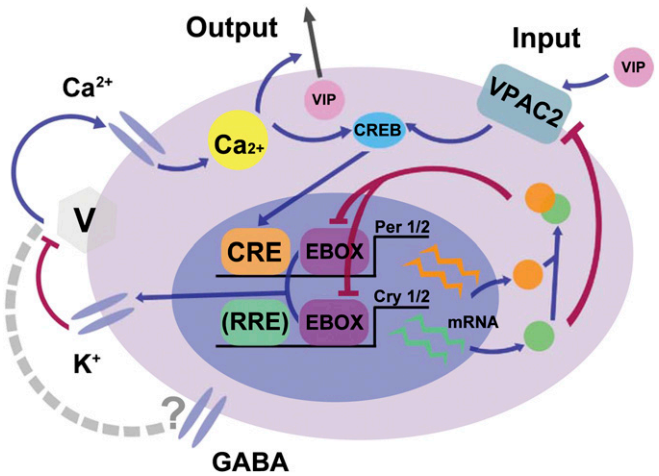


**Fig. 1.** Interactions between components of the SCN model. The full SCN model contains both a detailed molecular-clock model as well as a conductance-based electrophysiology model of the dynamics of each cell in the network. The connections between these components are highlighted here. The molecular-clock state, determined by E-box activity, influences the permeability of KCa and K–leak channels. These drive changes in membrane voltage, which affect intracellular calcium concentrations. Both calcium and VIP can lead to activation of CREB, causing transcription of *Per1* and *Per2*. Calcium also causes release of VIP in VIP-producing cells. The activity of the VPAC2 receptor is inhibited by CRY. GABA can lead to excitation or inhibition of membrane voltage depending on $E_{GABA}$.

**Experimental Measurement of the Spatial Distribution of Excited and Inhibited Cells.** The type of response of a cell to GABA is dependent on the chloride equilibrium potential of the cell ($E_{GABA}$), which is a function of the cell's intracellular chloride concentration. To estimate the relative GABA equilibrium potentials of cells in the SCN, we measure relative intracellular chloride levels by applying MQAE [N-(ethoxycarbonylmethyl)-6-methoxyquinolinium bromide] to acute SCN slices and measure fluorescence with a confocal microscope (Fig. 3*A*). MQAE is quenched by chloride, so the intracellular chloride concentration is assumed to be inversely proportional to the amount of fluorescence measured. A calibration of chloride quantification using MQAE can be found in *SI Appendix*, Fig. S1. Fluorescence is averaged over cell-sized regions (Fig. 3*B*) and used to estimate relative $E_{GABA}$ values across our model SCN (Fig. 3*C*), as described in *Materials and Methods*, which we scale to lie in a range between −32 and −80 mV, corresponding to chloride intracellular concentrations of roughly 47 mM and 7 mM, respectively, as has been previously reported (5, 10). Our own estimation of the intracellular chloride concentration and corresponding chloride reversal potential from 286 randomly selected cells from an SCN slice (*SI Appendix*, Fig. S1) finds chloride reversal potentials consistent with this range and distribution (between −70 and −40 mV). We find that our estimated $E_{GABA}$ values are roughly normally distributed (Fig. 3*D*) across the SCN, but that there is a spatial bias with more cells with higher $E_{GABA}$ in the dorsal SCN than in the ventral. The spatial distribution of relative chloride levels does not change over time (*SI Appendix*, Fig. S2). These findings suggest that subsets of cells are excited or inhibited throughout the entire circadian day, and the rest may change polarity as their resting membrane potential rises and falls above $E_{GABA}$.

**Predicted Consequences of Spatial Heterogeneity in GABA Signaling.** Using the distribution of $E_{GABA}$ from Fig. 3*C*, we simulate a network of 1,024 SCN neurons coupled through GABA alone. All molecular-clock parameters are taken from DeWoskin et al. (25) and additional electrophysiological parameters are from Diekman et al. (26). Heterogeneity is included in all parameters by drawing them from normal distributions with means equal to the fit values and SDs 2% of the means, representing unbiased heterogeneity between cells. Surprisingly, we find that GABA signaling seems to maintain some synchrony in the SCN, particularly within the GABA-excited subpopulation. Cells in the network that are strongly excited by GABA are better synchronized and have higher amplitude rhythms (Fig. 3*E*). Summaries of the circadian electrical activities over a single day for three sample cells are shown in Fig. 3 *F*–*H*, represented as the range of voltages attained by each cell continuously throughout the day. These cells have $E_{GABA}$ values such that they are always inhibited

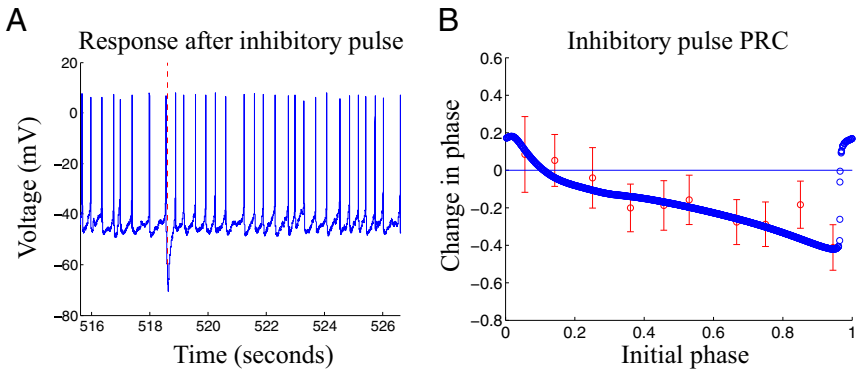


**Fig. 2.** Effects of inhibitory pulses on SCN neuron firing activity. (*A*) Sample firing activity of an SCN neuron before and after the administration of a hyperpolarizing pulse (time of pulse denoted by red dashed line). (*B*) The model predicted phase response curve (dark blue line) is plotted along with the mean and SE of responses to inhibitory pulses given experimentally to SCN neurons (red), binned by phase of pulse initiation (for the electrophysiology model, parameter $R = 2$). Both the model-predicted and experimentally determined responses show that the response to the pulse depends on when in the ISI it is given, with pulses given shortly after the firing of an action potential shortening the ISI (as in *A*), whereas pulses given late in the ISI lengthen it.

by GABA (−80 mV), inhibited at some times of day and excited at others (−60 mV), and always excited by GABA (−32 mV), respectively. These three cells represent the continuum of electrical activities seen in the model, with the trend that excitation by GABA can drive neurons to higher resting membrane voltages and consequently hyperexcitation, including the depolarized low-amplitude membrane oscillation and depolarized states that were described in Belle et al. (31). The model predicts that this causes higher amplitude rhythms in intracellular calcium (*SI Appendix*, Fig. S3), which can increase transcription and cause the higher amplitude molecular rhythms previously noted; this also leads to the hypothesis that GABA signaling could affect the synchrony of molecular rhythms by driving resting membrane voltage and consequently intracellular calcium rhythms.

The model predicts that because GABA signaling changes the firing activities of individual cells, it will also impact GABA release. To explore this idea, we compare the profile of GABA release across 1 day for the three cells shown in Fig. 3 *F–H* (plotted in *SI Appendix*, Fig. S4). Cells release large bursts of GABA after each action potential. This type of GABA release is termed phasic, and leads to the PSCs commonly described experimentally. During depolarization block, on the other hand, a very low level of GABA is predicted to be released at a roughly constant rate, lasting for some cells up to 4 or 5 h (*SI Appendix*, Fig. S4*C*). The magnitude of this release is less than 5% of the amplitude of GABA released after an action potential, but it is sustained over time. This type of sustained GABA release is similar to the tonic GABA release that has been seen experimentally in a variety of neuronal systems (32, 33) but not fully explored in SCN neurons.

**Tonic but Not Phasic GABA Signaling Effectively Shifts Molecular Rhythms.** To compare the effects of tonic and phasic GABA signaling on SCN neurons, we applied specific GABA time courses to simulated cells with GABA equilibrium potentials ranging between −80 and −32 mV. The first GABA stimulus used was a regular 10-Hz phasic GABA signal 5 h in duration, applied every 24 h. This mimics the signal a cell could receive from multiple upstream cells collectively firing 10 total action potentials per second between them, for 5 h/d. This signal caused no shift in the molecular rhythm of the downstream cell regardless of its $E_{GABA}$ (Fig. 4*A*), and regardless of when the window fell within the circadian day. The cells did not entrain to the signal. The second GABA stimulus applied was a 5-h window of tonic, low-amplitude GABA, given every 24 h, mimicking the GABA released by upstream cells entering depolarization block in the afternoon, e.g., around circadian time (CT) 3–8. Although a similar level of GABA was released with both signals, the tonic signal caused significant shifts in the molecular rhythms of the downstream cells, and the direction of the shift depended on the cell's $E_{GABA}$ (Fig. 4*B*). Cells were entrained by this signal with a fixed-phase relationship dependent on $E_{GABA}$.

To characterize this entrainment, we measure the response of individual SCN neurons in the network to this 5-h sustained GABA time course by calculating the PRC of sample cells with the most excitatory ($E_{GABA} = -32$ mV) or most inhibitory ($E_{GABA} = -80$ mV) responses to this signal. The PRC, shown in Fig. 4*C*, shows a stable steady state for the excited cells with the pulse beginning at around CT3. This matches exactly the time (~CT 3–8) when the tonic GABA is predicted to be released, when the excited cells enter the depolarized states (as in Fig. 3*H*), and also matches the phase of entrainment shown in Fig. 4*B* for the most excited cells. Conversely, cells inhibited by GABA have an unstable steady state at this time, flanked by regions of greatest advance and delay. If the sustained GABA pulse begins around this time, but not exactly at the steady state, cells will be pushed toward either big advances or delays, depending on their initial phase. The PRC predicts that the excited cells will stay synchronized, whereas the inhibited cells will split with some advancing and some delaying. Furthermore, it predicts that if this sustained signal persisted and was strong enough, the inhibited cells could synchronize as a secondary population antiphase to the GABA-excited cells.

**GABA Synchronizes Molecular Rhythms in Excited Cells.** We find that the distribution and percentage of cells within the network with fixed GABA polarities seem to have the most significant effects on synchrony of molecular rhythms. The cells that are always excited by GABA release tonic GABA when they become depolarized, and force cells that are strongly inhibited by GABA to shift antiphase to the tonic GABA signal. To further explore this in silico, we test idealized networks in which we consider only subpopulations of cells that are excited or inhibited at all times of day. For these populations, we fix the excited and inhibited GABA equilibrium potentials to −32 mV and −80 mV, respectively and vary the proportions of GABA-excited and GABA-inhibited cells in the network. To standardize the comparison, we begin all simulations with the same initial conditions and use three randomly drawn parameter sets for each network type.

In accordance with our own (Fig. 3), as well as previous experimental data (6, 8), we begin with 40% of the cells, specifically the dorsal shell region, excited by GABA, and the remaining 60% inhibited by GABA. Starting with the cells in an initially synchronized state, we simulate the network and monitor PER2

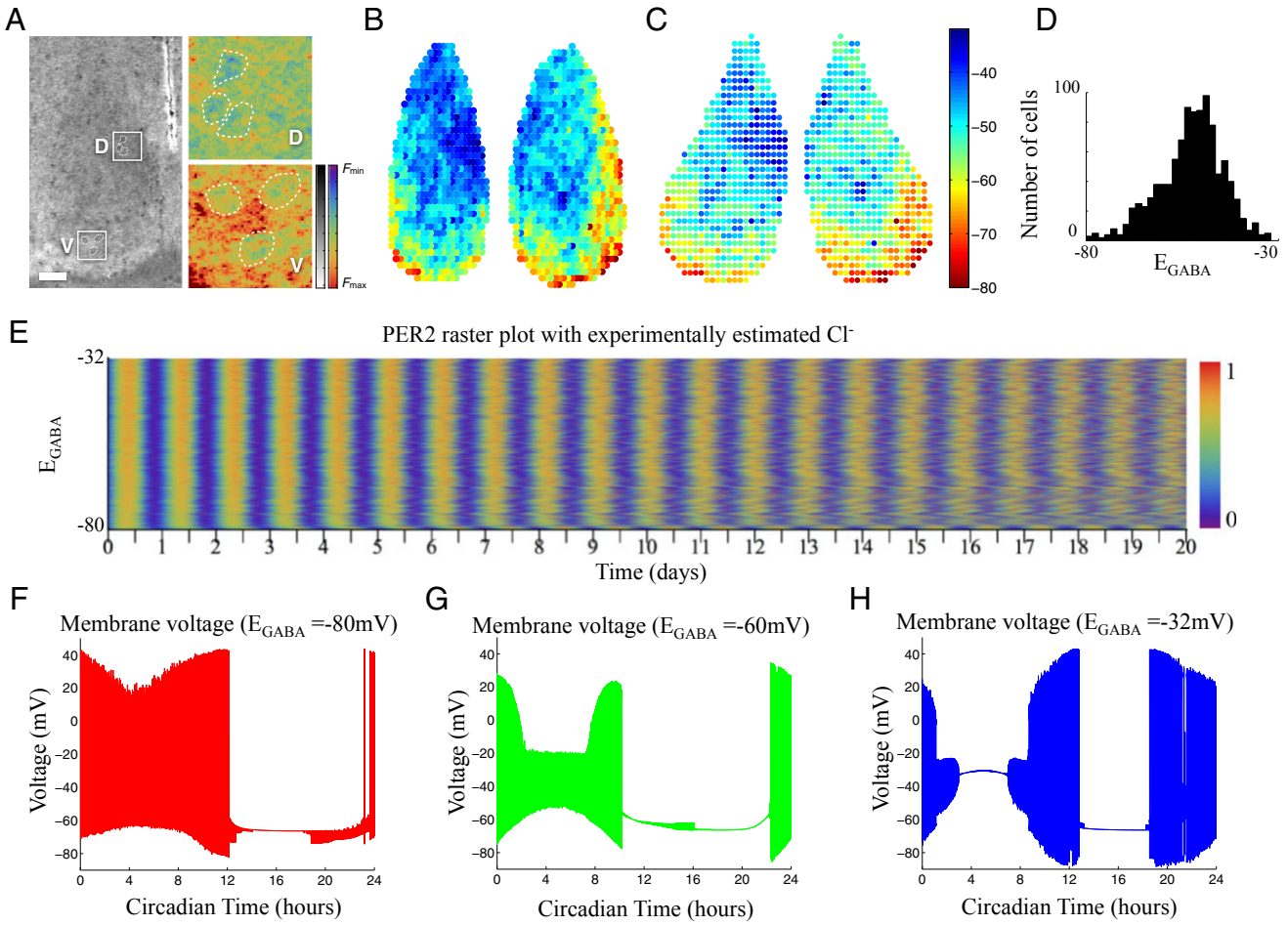


**Fig. 3.** Experimentally measured intracellular chloride is used to determine $E_{GABA}$ for simulations, leading to predictions of strong effects of GABA signaling on cellular electrical activity rhythms. (*A*) Confocal microscopy of MQAE fluorescence in a unilateral SCN from an acute slice. (Scale bar, 100 μm.) MQAE is quenched by chloride, so areas with high fluorescence represent low intracellular chloride. Magnified images of cell bodies in dorsal, D, cells show lower fluorescence than those in ventral, V, cells. (*B*) Fluorescence values from the whole SCN slice are averaged over cell-sized regions, and (*C*) used to estimate the relative distribution of $E_{GABA}$. Cells with high $E_{GABA}$ are excited by GABA, and with low $E_{GABA}$ are inhibited by it. Note that cells are plotted on a grid for visualization purposes only and that connectivity is determined independently of distance between cells, as described in the methods. (*D*) Estimated $E_{GABA}$ levels across the SCN are found to be roughly normally distributed but with a clear spatial bias between the dorsal and ventral SCN. (*E*) A raster plot of simulated PER2 rhythms over 20 d for an SCN with the experimentally estimated $E_{GABA}$ values from *C* (cells are sorted by $E_{GABA}$). (*F*–*H*) Circadian variation in electrical activity for sample cells with $E_{GABA}$ values of −80 mV (*F*), −60 mV (*G*), and −32 mV (*H*), plotted as the range of voltages attained by the cells throughout the day. Circadian time is determined relative to the peak in whole SCN PER2 protein levels, which is defined to be CT12.

levels over time, as is often done experimentally. Fig. 5*A* shows snapshots of PER2 rhythms on the 10th day of simulated time, from which it is clear that the GABA-excited cells in the dorsal shell have maintained better synchrony in comparison with the GABA-inhibited ventral core where cells appear to be at all phases. A movie of the full simulation can be found in Movie S1. Raster plots from this video (Fig. 5*B*) clearly show that the cells excited by GABA (sorted to the top of the raster plot) have higher amplitude rhythms, and are better synchronized as one cluster, whereas the cells inhibited by GABA (at the bottom) begin to free run and desynchronize over time. This simulation agrees with the role for GABA signaling in synchronizing the excited cells and desynchronizing the inhibited cells proposed above.

The inhibitory GABA cells desynchronize from the synchronized excitatory GABA population, and can achieve an opposite phase if a strong enough signal is sent from the excitatory GABA population. This is shown in a random network with a 60:40 proportion of excited to inhibited cells in Fig. 6*A*, and for an 80:20 excited:inhibited random network in *SI Appendix*, Fig. S5*A*. Each of these simulations used a 10% random connectivity for GABAergic synapses in the network, but consistent results are also seen if a small-world connectivity is used. Additional raster plots (*SI Appendix*, Fig. S5 *B* and *C*) with small-world connectivity show that synchrony is maintained in the GABA-excited population, but that the GABA-inhibited population does not synchronize in antiphase. Because the number of connections from the excited to the inhibited subpopulation is low in the small-world networks, the tonic signal is not strong enough to force the inhibited population to the antiphase configuration. The process of this antiphase synchronization in a 60:40 excited: inhibited random network is demonstrated in Fig. 6*B*, which shows Rayleigh plots depicting the phases of mean PER2, calcium, and firing-rate rhythms of the excited (blue) and inhibited (red) populations on days 5, 10, and 20 after the beginning of the simulation, relative to the phase of the mean PER2 level across all cells (black). At 5 d the three rhythms are separated in phase, with roughly the same phase relationships in both the excited and inhibited populations. By day 10 the calcium rhythm in the inhibited cells has shifted to be antiphase to that of the excited cells, and by day 20 the phase of the PER2 rhythm in the

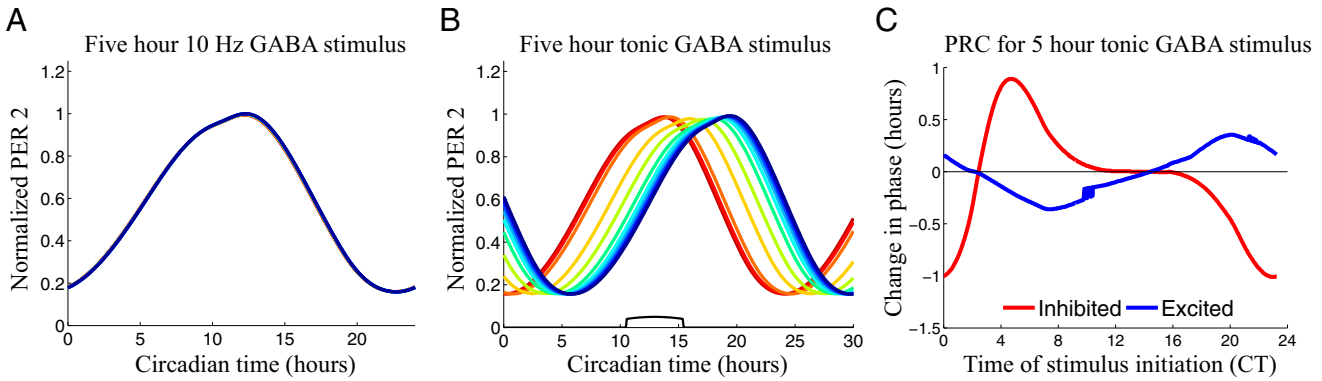


**Fig. 4.** Tonic but not phasic GABA causes shifts in PER2 rhythms, with different phasing depending on the cell's GABA equilibrium potential. Cells with $E_{GABA}$ ranging from −80 (red) to −32 (blue) are stimulated with 5 h of phasic GABA at 10 Hz (*A*) or low-level tonic GABA (*B*); GABA equilibrium potentials denoted by colors as in Fig. 3*C*. PER2 rhythms for cells in *A* overlap, showing that 5 h of phasic GABA does not shift the molecular rhythms of any of the cells, and they do not entrain to it regardless of when in the cycle it is given. Cells do shift to entrain to the tonic GABA stimulus with the phase relationships shown in *B*. The timing and relative amplitude of the GABA stimulus are denoted by the black curve. (*C*) A PRC of strongly inhibited ($E_{GABA}$ = −80) and excited ($E_{GABA}$ = −32) cells in response to the 5-h tonic GABA stimulus. Initial phase is defined as the time of the beginning of the stimulus and for each cell, circadian time is determined relative to the peak in the cell's PER2 protein levels, which is defined to be CT12.

inhibited cells has followed suit. Note that the firing-rate rhythms of both populations are, however, still in phase. This illustrates that the molecular, calcium and electrophysiological rhythms need not show the same phase relationship.

**The Combined Effects of VIP and GABA.** VIP is a well-known SCN intercellular signal and we have previously studied its role in synchronizing the molecular clocks of SCN neurons (25). We now use our integrated model, including cellular electrophysiology and GABA signaling, to investigate the effects of having no GABA or different balances between excitatory and inhibitory GABA within the VIP-coupled SCN network. The subset of cells that produce and release VIP is determined by immunohistochemistry (*SI Appendix*, Fig. S6*A*) and denoted in the model SCN

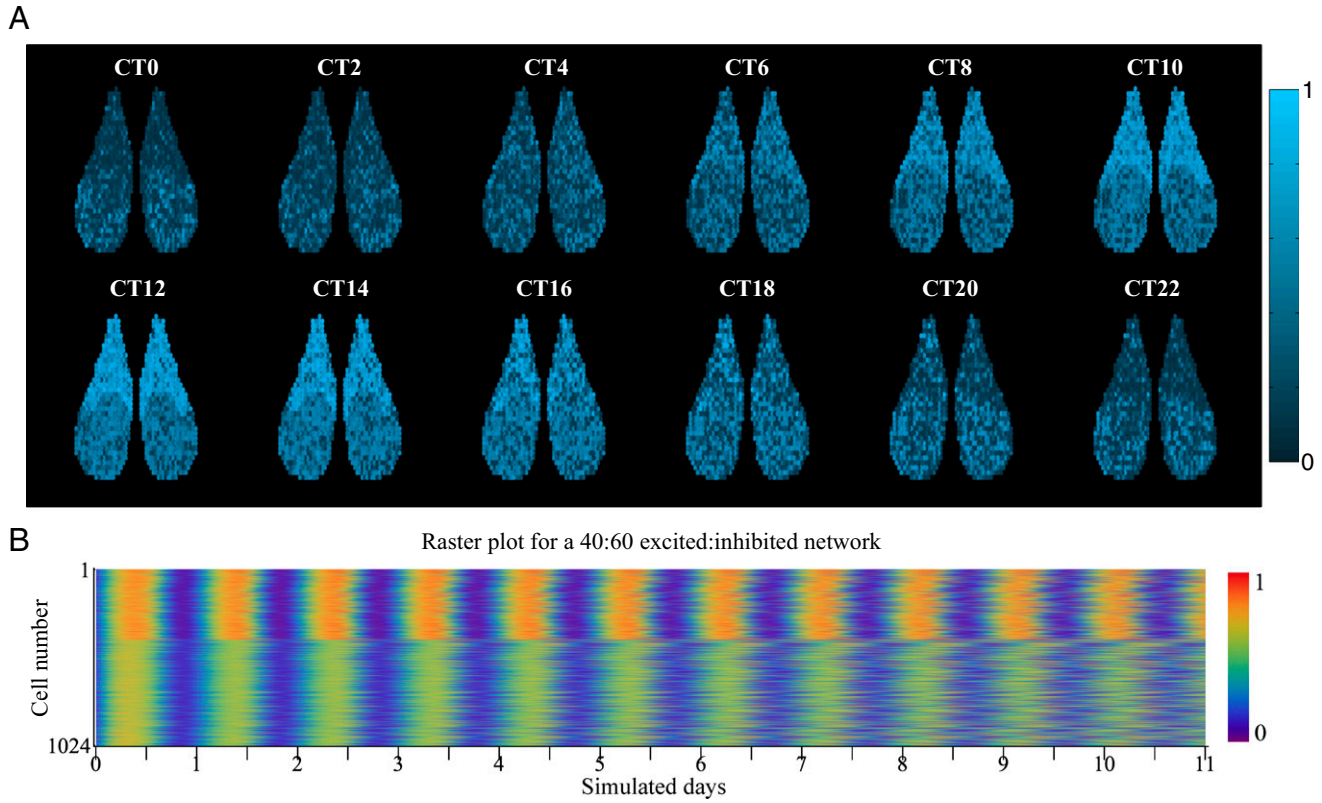


**Fig. 5.** Cells excited by GABA retain synchrony over time. (*A*) Snapshots of PER2 rhythms in a simulated SCN every 2 h over the 10th day of simulated time (CT0 to CT22 from left to right, top to bottom, all values normalized by the maximum value in the simulation). A movie of the full simulation can be found in Movie S1. The cells excited by GABA, located in the dorsal shell region, form a clear cluster. Circadian time is determined relative to the peak in whole SCN PER2 protein levels, which is defined to be CT12. (*B*) A raster plot of PER2 rhythms for the full 11-d simulation. Cells excited by GABA are sorted to the top, and can be seen to retain synchrony better over time whereas those inhibited by GABA desynchronize. Color bars for each scale are shown on the right.

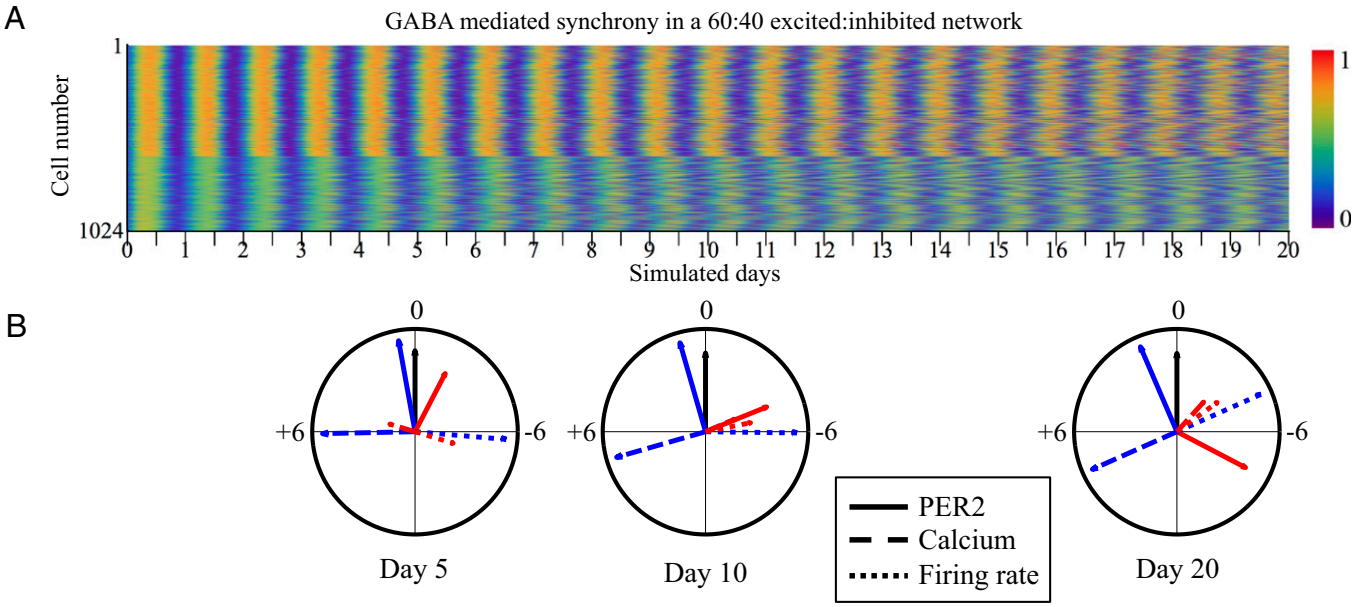


**Fig. 6.** Random networks with large fractions of cells excited by GABA form excited and inhibited clusters in antiphase, driven by calcium. (*A*) A raster plot of normalized PER2 rhythms in a network with 60% cells excited by GABA shows the formation of two clusters, one with the excited cells and one with the inhibited. These clusters increase in coherence as the percentage of excited cells is increased (*SI Appendix*, Fig. S5). (*B*) The formation of these clusters can be seen in Rayleigh plots of the mean PER2 (solid line), calcium (dashed line), and firing rate (dotted line) rhythms for the excited (blue) and inhibited (red) populations. At day 5, each of the three rhythms has the same phasing in both populations. By day 10, however, tonic GABA signaling pushes the inhibited calcium rhythm to antiphase of the excited calcium rhythm, and by day 20, the PER2 rhythm has followed as well. All phases are relative to the total SCN PER2 protein rhythm (black), and are determined as the difference in hours between the trough of the rhythm and the trough of the global PER2 rhythm (positive numbers are advanced and negative delayed).

in *SI Appendix*, Fig. S6*B* in green. Raster plots from individual simulations are shown in *SI Appendix*, Fig. S7. The combined effects of VIP and GABA remove the clustering of the GABA-inhibited or GABA-excited cells. Additionally, removing GABA causes a tighter distribution of phases in agreement with Freeman et al. (6) and Myung et al. (15). Most importantly, increasing the concentration of excitatory GABA cells in the network yields a larger phase distribution, in agreement with previous experimental results (Fig. 7) (8, 11, 12). These findings lead to the prediction that the SCN can vary the fraction of cells with different GABA polarities as a mechanism for regulating the degree of synchrony in the network. Additionally, these differences affect the ability of the SCN network to phase shift. Model-predicted PRCs for the application of 5 h of tonic GABA to the SCN network are shown in *SI Appendix*, Fig. S8. The PRCs match the shape and phasing of the experimentally found PRC to the $GABA_A$ receptor agonist muscimol (34), but differ in amplitude depending on the balance of GABA-excited and -inhibited neurons.

**GABA Controls Tissue-Level Electrical Activity.** In addition to its effect on the synchrony of molecular rhythms, GABA has a strong effect on electrical activity. In particular, changing the proportion of excited to inhibited cells in the network changes the amplitude and timing of firing-rate rhythms. An example video showing the electrical activity of a network with a 40:60 balance of GABA-excited:inhibited neurons at four circadian times is provided in Movie S2. The model predicts that networks with small fractions of excited cells will have a single peak in firing rhythms around CT6, but networks with higher percentages of excited cells can actually show a crepuscular firing pattern with peaks around both dawn and dusk (Fig. 8*A*). This type of pattern has been seen before experimentally in *Per1*::eGFP cells in mice (31). This was also found when hamster SCN were sliced horizontally (35, 36) but not coronally. Thus, our model provides a possible explanation: horizontal slices of hamster SCN could contain a higher fraction of GABA-excited neurons than coronal slices.

Separating out the contributions of the excited and inhibited neurons in Fig. 8 *B* and *C*, respectively, we find that both subsets can show either unimodal or bimodal firing patterns depending on the balance of excited to inhibited neurons in the network. In most networks, each subpopulation is more likely to have unimodal

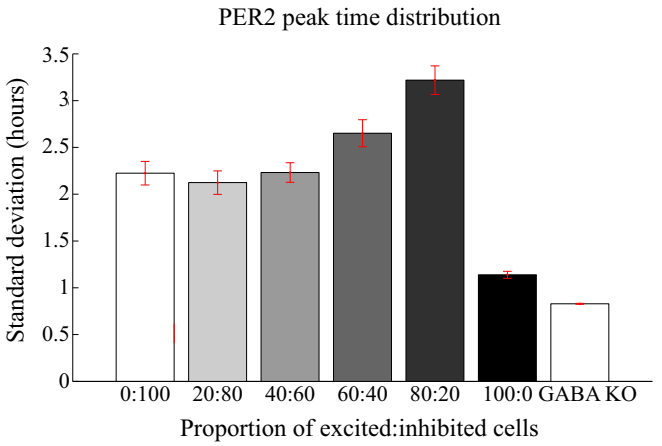


**Fig. 7.** SD of the PER2 peak time distribution as a function of the proportion of GABA-excited to GABA-inhibited cells (E:I) in the network. Mean values and SEs for three networks with different randomized parameters are shown for each network type. Cells are best synchronized and most in phase in the network where either 100% of cells are excited by GABA or when GABA is knocked out. Networks with E:I proportions between 20:80 and 80:20 are less in phase, with increasing numbers of excited cells leading to increased variance in the distribution of phases in the network. Entirely inhibitory networks (0:100) rank in between the 40:60 and 60:40 networks.

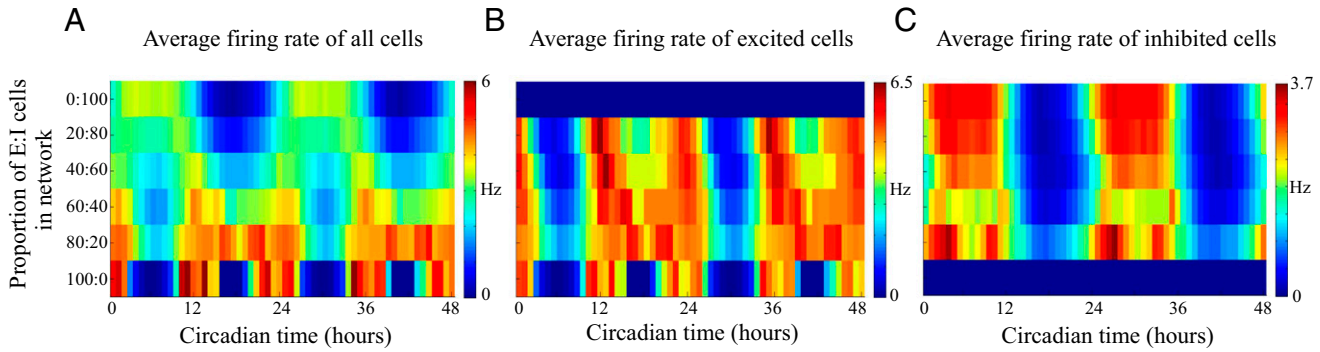


**Fig. 8.** Rhythms in firing rate differ in amplitude and phasing depending on the proportion of excited to inhibited cells in the network. (*A*) Networks with large fractions of GABA-inhibited neurons are unimodal and those with large fractions of excited neurons can show bimodal, crepuscular firing patterns. The excited (*B*) and inhibited (*C*) subsets can each show either of these patterns depending on the balance of excited to inhibited neurons in the network. Circadian time is determined relative to the peak in whole SCN PER2 protein levels, which is defined to be CT12.

firing if it is in the majority, and drive neurons with the opposite polarity to fire before or after this peak. The one exception is the entirely excitatory network (100:0), which shows crepuscular firing. These plots show that the timing of SCN firing rhythms can be modulated by changing the excitation/inhibition balance in the network, and thus can be shifted to have different phase relationships relative to the molecular clock, without compromising synchrony of the molecular rhythms.

## Discussion

The model developed and tested here provides a framework for studying the complex interactions between the molecular and electrical activities of individual SCN neurons, as well as the synchrony and phase relationships seen within the network. In particular, it is the perfect tool for investigating the conflicting hypotheses about the role of GABA signaling in the SCN. Here we propose a new mechanism that could help to explain some of the paradoxical results.

We find that GABA signaling in the SCN has two components. Large quantities of GABA are released transiently following action potentials (phasic release). Additionally, a subset of neurons becomes depolarized, and releases a sustained low level of GABA (tonic release). The essential assumption of the model that leads to this prediction is that GABA release is a function of a neuron's membrane voltage. This finding implies that if cells become hyperexcited and depolarized enough, they can release low levels of GABA even without firing action potentials. Our model predicts, and experiments confirm, that pulsatile GABA can both increase and decrease the firing of a cell, depending on when during the ISI it is provided. As the tonic GABA signal occurs both during the phases that increase and the phases that decrease the ISI, and also occurs at a low overall level, it does not significantly affect firing rate. However, it does set the overall depolarization of a neuron, which our model—as well as previous studies (26)—predicts will set the intracellular calcium level, and can trigger transcription.

Remarkably, this process allows the electrical firing of a neuron to become decoupled from its molecular rhythms. Tonic GABA can affect the molecular circadian clock, but this signal, we predict, comes only from a subset of neurons that have achieved a high level of depolarization. This depolarization could be because of signaling from their internal molecular clock, depolarization from long-lasting neurotransmitters like glutamate, which transmit information from the retina or GABA itself. The phasic GABA signal, on the other hand, does not affect molecular rhythms. We hypothesize that this could be important for SCN output, as neurons in the SCN could fire action potentials to transmit an output signal without shifting their own internal timekeeping. Furthermore, it allows tonic and phasic GABA to be separately regulated.

These results raise the interesting question of whether coordinated firing or many phasic GABAergic signals could act like the tonic GABA signal and shift the molecular clock. Although theoretically many phasic GABA PSCs could accumulate to give an effect similar to the tonic GABA signal, we find that the number, frequency, and strength of these PSCs would have to be much greater than that previously reported (29). Because of GABA's relatively fast clearance, it would require constant stimulation by many upstream cells to obtain the same persistent GABA levels produced by the tonic signal, but because of sparse connectivity (6, 37) and irregular firing patterns (29), this does not happen in the model. Interestingly, a recent study found large phase shifts when many SCN neurons were optogenetically stimulated in unison with an 8-Hz signal for 1 h to mimic the firing of action potentials at 8 Hz (38). To study this in our model, we incorporate a channelrhodopsin (ChR2)-like current into our electrophysiological model, taking parameters from a previously published model of optogenetic stimulation of ChR2 (39), and simulate this stimulus (details of the methods are given in *SI Appendix*). Surprisingly, we find a PRC to this stimulus that is remarkably close to that reported experimentally (*SI Appendix*, Fig. S9). We find that the important difference between optogenetic stimulation and phasic GABA signaling lies in the duration of the signal. The optogenetic stimuli each lasted 10 ms and ChR2 has an estimated decay constant of 15 ms (39). The phasic GABA pulse, on the other hand, lasted only about 5–6 ms with a much shorter decay constant of 5.6 ms. Because ChR2 causes a more sustained increase in voltage and is directly permeable to calcium (40, 41), it causes a much greater increase in intracellular calcium and is therefore effective in shifting the molecular clock, whereas the phasic GABA signal is not. Thus, although we find certain kinds of oscillatory electrical activity can cause calcium influx and shift the molecular clock in a similar way to the tonic GABA signal, the irregular firing of average SCN neurons that causes phasic GABA release does not.

Using the tonic GABA signal, we predict that the GABA-excited cells can work together to send off a synchronizing signal to each other, and one that can push the phase of the inhibited cells away. What matters most in generating a synchronizing signal is the depolarization of the neuron, so factors besides GABA are also important. If this signal arrives before the normal calcium rise in the cell (which begins around CT3), it will advance the rhythm in excitatory cells, and delay it in inhibitory cells. If it occurs after this calcium rise, the opposite will be seen. As calcium is at low levels from dusk through midnight, GABA

has less effect during these phases. This finding matches what is seen in PRCs, and what is predicted by our model.

For these reasons, it is not surprising that another coupling agent, VIP, is strongly active in the SCN. In the presence of VIP and GABA, our model predicts the surprising result that has been seen experimentally: that GABA can synchronize or desynchronize neurons in a normally functioning SCN. We add to this the fact that this effect is strongest when a combination of excitatory and inhibitory GABA is present. Only inhibitory or only excitatory GABA yields a more phase-synchronized SCN. Surprisingly, small changes in the proportion of excited to inhibited cells can change the synchrony of the SCN, indicating this balance could be tweaked for regulation of circadian rhythms. In particular, this has interesting applications to the study of day-length encoding in the SCN. Previous studies have shown an increase in excitation in the SCN (11), and a reorganization of the phases of SCN neurons in animals entrained under long days (12, 15, 42). These observations are both consistent with the model predictions presented here, and are further explored in a companion article using this model (43).

Our work presents a different view of synchronization in the SCN that depends not only on the specific connectivity of the network, but also depends highly on the form of the signal produced. We propose that small subsets of SCN neurons (e.g., the 10% that release VIP or a small set of excitatory neurons) are actually responsible for producing the signals that affect synchrony. This is different from the hypothesis that all SCN neurons contribute to synchrony, and that the large number of neurons reduces noise (44, 45). We predict that potentially most of the neurons in the SCN and the majority of the GABA signaling (the phasic portion) do not contribute to synchrony (e.g., to reduce noise), but instead generate a large variety of firing patterns, including bimodal or crepuscular patterns, that are likely important for the SCN output. The specifics and timing of neuronal firing certainly depend on synaptic connectivity, but we find that this firing does not affect synchrony. This provides a potential answer to the question of how SCN neurons are able to show a large variety of electrical activities and generate outputs for the rest of the body without desynchronizing their own rhythms. Such mechanisms are likely found in other parts of the brain and allow neurons to change their molecular, gene expression or biochemical state in response to some signals, while allowing neuronal processing to simultaneously occur unhindered.

## Materials and Methods

**Model Formulation.** The model presented here integrates previously published detailed models of the molecular clock (24, 25) and electrophysiology (26) of SCN neurons into an SCN network model. All SCN network simulations presented use 1,024 cells. Because our measurements of $E_{GABA}$ values and the VIP producing region come from SCN slices with slightly different shapes, we chose a single SCN image as the model for our SCN grid, based on figure 2 of ref. 27. We then found parameters for grid cells by overlaying the grid on top of SCN slice measurements and choosing values from the closest cells in the SCN slice. The grid is for visualization purposes only and not representative of connectivity, which is described below, but rather is meant to display behavior from representative cells across the SCN.

For full descriptions of all model components, see *SI Appendix*. The electrophysiology and molecular-clock models are coupled together bidirectionally. The phase of the molecular clock affects two ionic conductances ($g_{KCa}$ and $g_{K-leak}$ as in ref. 26), with $g_{KCa} = 198.0/[1.0+\exp(R)]+2.0$ and $g_{K-leak} = 0.2/[1.0+\exp(R)]$, where $R = clk \times 11.36 \times (G - 0.25)$, where $G$ is the activity of the E-box and $clk$ is a parameter that determines the strength of the influence of the molecular clock on the electrical activity of the cell ($clk = 2.2$). Conversely, a cell's electrophysiology affects its molecular clock through intracellular calcium in two ways. First, in VIP-producing cells, VIP is assumed to be released at a rate proportional to a cell's intracellular calcium concentration: $6{,}000 \times vpr \times (Ca_c)$, where $Ca_c$ is the cytosolic calcium concentration. This is based on the assumption that exocytosis of VIP-containing vesicles is calcium dependent, and also leads to the proper phasing of CRE activity. Second, calcium can lead to the phosphorylation of CREB in a VIP-independent manner. The updated ODE for CREB activity from ref. 25 becomes $d(\text{CREB})/dt = 6{,}500 \times Ca_c + vs \times \text{cAMP} - us \times \text{CREB}$. Only a subset of SCN neurons release VIP (*SI Appendix*, Fig. S6*B*), and it is assumed to diffuse quickly across the SCN so that the connectivity is some to all.

The model of GABA signaling is adapted from Ermentrout and Terman (46). We set $g_{GABA}$ to 0.5 and $K_P$ to 3 mV to create postsynaptic currents of the same magnitude and duration, as those seen in the SCN (29), and changed $V_T$ to −20 mV. Additionally, we varied the GABA equilibrium potential, $E_{GABA}$, based on our chloride measurements using MQAE, as noted in the text. Synaptic connectivity in the SCN is assumed to be sparse in accordance with experimental data (6). All simulations presented here assume 10% random connectivity of GABAergic synapses unless otherwise noted. The synaptic input to each cell is normalized by the number of upstream connections that cell receives, so that the synaptic drive to each cell in the network is on the same order regardless of the exact number of upstream cells signaling to it. Full explanations of the models used, including a reproduction of the equations of the GABA signaling model, can be found in *SI Appendix*.

All parameters for the molecular-clock model as well as two of the electrophysiology parameters ($E_{Ca}$ and $clk$) are drawn from a normal distribution with means equal to the previously fit values (25, 26) and SD 2% of the mean. This is done to allow for unbiased intercellular heterogeneity in amplitude and period, and is based on previous estimates of biochemical parameter heterogeneity in the SCN (14). The model is deterministic and does not include intrinsic stochasticity, as has been done in some other modeling studies (14, 47). Certainly much could be learned from studying stochasticity in this context as well, but here we first study different types of GABA signals generated by a heterogeneous population and their effects on synchrony. Details on the numerical methods used for simulating the model on GPUs and their accuracy can be found in *SI Appendix* (including *SI Appendix*, Figs. S10 and S11).

**Hyperpolarizing Current Phase-Response Measurements.** Electrophysiological recordings were done as in Belle et al. (31). Experimental procedures were carried out according to the provisions of the UK Animal (Scientific Procedures) Act 1986. Ten-picoamps hyperpolarizing current pulses, 60 ms in duration, were applied to SCN neurons in acute mouse brain slices. The $GABA_A$ receptor antagonist gabazine (29) was used to block the effects of endogenous synaptic input. Only neurons that repetitively fired both before and after the pulse were used. A cell's characteristic ISI was measured as the mean of the lengths of the four ISIs before each pulse. Change in phase was determined as the difference in timing of the third subsequent spike after the pulse and the predicted time of this spike if no pulse had been given (three standard ISIs after the spike preceding the pulse).

**MQAE Imaging of Intracellular Free Chloride Concentration.** Wild-type C57BL/6J mice (SLC Japan) were maintained under 12-h light and 12-h dark conditions under constant environmental temperature. The animal experiment protocols were approved by the Animal Research Committee of RIKEN Brain Science Institute. Coronal brain slices of 140- to 150-μm thickness were prepared from postnatal day 20- to 30-d-old mice using a vibratome (DSK Japan) in ice-cold HBSS. The SCN was dissected from the slice under the surgical microscope and transferred to the culture membrane (Millicell, Millipore) in a sealed 35-mm dish containing 1 mL of DMEM culture medium supplemented with B27 as in Myung et al. (15). One milliliter of the fluorescent dye MQAE (Molecular Probes) was added to the medium and incubated for 2–3 h at 37 °C. Time-lapse MQAE fluorescence images from the SCN were obtained with a confocal microscope (FV1000, Olympus) under sequential 405-nm and 488-nm excitations with Kalman filtering in ∼10 $z$-axis stacks through 10× and 20× objectives (Olympus). Images were saved in TIFF format and later analyzed with ImageJ (NIH), Mathematica, and Matlab. Time-lapse imaging was done in 30-min intervals, and the nuclear signal from the green emission (from the 488-nm excitation) was used to identify regions-of-interest where chloride was then estimated from the blue emission (405-nm excitation).

**Identification of VIP-Producing Cells.** VIP immunostaining was performed on SCN slices from animals pretreated with colchicine (10 μg/μK) by intracerebroventricular injection and fixed-trough cardiac perfusion after pentobarbital anesthesia. Cryosections of the SCN were prepared and immunohistochemistry against VIP was performed as in Myung et al. (15). VIP rabbit polyclonal antibody (ImmunoStar) was used at 1:1,000 dilution.

**ACKNOWLEDGMENTS.** We thank Santiago Schnell for helpful discussions and computing resources, Seth Meyer for technical support and assistance with

graphics processing unit computing, Olivia Walch for help with Fig. 1, and Adam Stinchcombe for many helpful conversations regarding the numerical methods used to solve the model. This work was supported by Human Frontiers of Science Program Grant RPG 24/2012; Air Force Office of Scientific Research Grant FA 9550-14-1-0092 (to D.D. and D.B.F.); RIKEN Incentive Research Project Grant G1E-54500 (to J.M.); Ministry of Education, Culture, Sports, Science and Technology in Japan Grants-in-Aid for Scientific Research and CREST from the Japan Science and Technology Agency (T.T.); and Biotechnology and Biological Sciences Research Council UK Project Grant BB/L007665 and Wellcome Trust Project Grant WT092319MA (to H.D.P. and M.D.C.B.). This work used the Extreme Science and Engineering Discovery Environment, which is supported by National Science Foundation Grant ACI-1053575.

1. Maywood ES, et al. (2011) Tuning the period of the mammalian circadian clock: Additive and independent effects of CK1εTau and Fbxl3Afh mutations on mouse circadian behavior and molecular pacemaking. *J Neurosci* 31(4):1539–1544.
2. Maywood ES, Chesham JE, O'Brien JA, Hastings MH (2011) A diversity of paracrine signals sustains molecular circadian cycling in suprachiasmatic nucleus circuits. *Proc Natl Acad Sci USA* 108(34):14306–14311.
3. Moore RY, Speh JC (1993) GABA is the principal neurotransmitter of the circadian system. *Neurosci Lett* 150(1):112–116.
4. Liu C, Reppert SM (2000) GABA synchronizes clock cells within the suprachiasmatic circadian clock. *Neuron* 25(1):123–128.
5. Alamilla J, Perez-Burgos A, Quinto D, Aguilar-Roblero R (2014) Circadian modulation of the $Cl^-$ equilibrium potential in the rat suprachiasmatic nuclei. *BioMed Res Int* 2014: 424982.
6. Freeman GM, Jr, Krock RM, Aton SJ, Thaben P, Herzog ED (2013) GABA networks destabilize genetic oscillations in the circadian pacemaker. *Neuron* 78(5):799–806.
7. Choi HJ, et al. (2008) Excitatory actions of GABA in the suprachiasmatic nucleus. *J Neurosci* 28(21):5450–5459.
8. Albus H, Vansteensel MJ, Michel S, Block GD, Meijer JH (2005) A GABAergic mechanism is necessary for coupling dissociable ventral and dorsal regional oscillators within the circadian clock. *Curr Biol* 15(10):886–893.
9. De Jeu M, Pennartz C (2002) Circadian modulation of GABA function in the rat suprachiasmatic nucleus: Excitatory effects during the night phase. *J Neurophysiol* 87(2): 834–844.
10. Wagner S, Castel M, Gainer H, Yarom Y (1997) GABA in the mammalian suprachiasmatic nucleus and its role in diurnal rhythmicity. *Nature* 387(6633):598–603.
11. Farajnia S, van Westering TLE, Meijer JH, Michel S (2014) Seasonal induction of GABAergic excitation in the central mammalian clock. *Proc Natl Acad Sci USA* 111(26):9627–9632.
12. Evans JA, Leise TL, Castanon-Cervantes O, Davidson AJ (2013) Dynamic interactions mediated by nonredundant signaling mechanisms couple circadian clock neurons. *Neuron* 80(4):973–983.
13. Ralph MR, Menaker M (1985) Bicuculline blocks circadian phase delays but not advances. *Brain Res* 325(1-2):362–365.
14. Ko CH, et al. (2010) Emergence of noise-induced oscillations in the central circadian pacemaker. *PLoS Biol* 8(10):e1000513.
15. Myung J, et al. (2012) Period coding of Bmal1 oscillators in the suprachiasmatic nucleus. *J Neurosci* 32(26):8900–8918.
16. Aton SJ, Huettner JE, Straume M, Herzog ED (2006) GABA and Gi/o differentially control circadian rhythms and synchrony in clock neurons. *Proc Natl Acad Sci USA* 103(50):19188–19193.
17. Bernard S, Gonze D, Cajavec B, Herzel H, Kramer A (2007) Synchronization-induced rhythmicity of circadian oscillators in the suprachiasmatic nucleus. *PLOS Comput Biol* 3(4):e68.
18. Gonze D, Bernard S, Waltermann C, Kramer A, Herzel H (2005) Spontaneous synchronization of coupled circadian oscillators. *Biophys J* 89(1):120–129.
19. To T-L, Henson MA, Herzog ED, Doyle FJ, 3rd (2007) A molecular model for intercellular synchronization in the mammalian circadian clock. *Biophys J* 92(11):3792–3803.
20. Relógio A, et al. (2011) Tuning the mammalian circadian clock: Robust synergy of two loops. *PLOS Comput Biol* 7(12):e1002309.
21. Leloup J-C, Goldbeter A (2003) Toward a detailed computational model for the mammalian circadian clock. *Proc Natl Acad Sci USA* 100(12):7051–7056.
22. Vasalou C, Herzog ED, Henson MA (2011) Multicellular model for intercellular synchronization in circadian neural networks. *Biophys J* 101(1):12–20.
23. Vasalou C, Henson MA (2010) A multiscale model to investigate circadian rhythmicity of pacemaker neurons in the suprachiasmatic nucleus. *PLOS Comput Biol* 6(3):e1000706.
24. Kim JK, Forger DB (2012) A mechanism for robust circadian timekeeping via stoichiometric balance. *Mol Syst Biol* 8:630.
25. DeWoskin D, Geng W, Stinchcombe AR, Forger DB (2014) It is not the parts, but how they interact that determines the behaviour of circadian rhythms across scales and organisms. *Interface Focus* 4(3):20130076.
26. Diekman CO, et al. (2013) Causes and consequences of hyperexcitation in central clock neurons. *PLOS Comput Biol* 9(8):e1003196.
27. An S, Tsai C, Ronecker J, Bayly A, Herzog ED (2012) Spatiotemporal distribution of vasoactive intestinal polypeptide receptor 2 in mouse suprachiasmatic nucleus. *J Comp Neurol* 520(12):2730–2741.
28. Zhang EE, et al. (2010) Cryptochrome mediates circadian regulation of cAMP signaling and hepatic gluconeogenesis. *Nat Med* 16(10):1152–1156.
29. Kononenko NI, Dudek FE (2004) Mechanism of irregular firing of suprachiasmatic nucleus neurons in rat hypothalamic slices. *J Neurophysiol* 91(1):267–273.
30. Sim CK, Forger DB (2007) Modeling the electrophysiology of suprachiasmatic nucleus neurons. *J Biol Rhythms* 22(5):445–453.
31. Belle MDC, Diekman CO, Forger DB, Piggins HD (2009) Daily electrical silencing in the mammalian circadian clock. *Science* 326(5950):281–284.
32. Lee S, et al. (2010) Channel-mediated tonic GABA release from glia. *Science* 330(6005): 790–796.
33. Farrant M, Nusser Z (2005) Variations on an inhibitory theme: Phasic and tonic activation of $GABA_A$ receptors. *Nat Rev Neurosci* 6(3):215–229.
34. Smith RD, Inouye S, Turek FW (1989) Central administration of muscimol phase-shifts the mammalian circadian clock. *J Comp Physiol A Neuroethol Sens Neural Behav Physiol* 164(6):805–814.
35. Jagota A, de la Iglesia HO, Schwartz WJ (2000) Morning and evening circadian oscillations in the suprachiasmatic nucleus in vitro. *Nat Neurosci* 3(4):372–376.
36. Burgoon PW, Lindberg PT, Gillette MU (2004) Different patterns of circadian oscillation in the suprachiasmatic nucleus of hamster, mouse, and rat. *J Comp Physiol A Neuroethol Sens Neural Behav Physiol* 190(2):167–171.
37. Fan J, et al. (2015) Vasoactive intestinal polypeptide (VIP)-expressing neurons in the suprachiasmatic nucleus provide sparse GABAergic outputs to local neurons with circadian regulation occurring distal to the opening of postsynaptic $GABA_A$ ionotropic receptors. *J Neurosci* 35(5):1905–1920.
38. Jones JR, Tackenberg MC, McMahon DG (2015) Manipulating circadian clock neuron firing rate resets molecular circadian rhythms and behavior. *Nat Neurosci* 18(3):373–375.
39. Williams JC, et al. (2013) Computational optogenetics: Empirically-derived voltage- and light-sensitive channelrhodopsin-2 model. *PLOS Comput Biol* 9(9):e1003220.
40. Nagel G, et al. (2003) Channelrhodopsin-2, a directly light-gated cation-selective membrane channel. *Proc Natl Acad Sci USA* 100(24):13940–13945.
41. Caldwell JH, et al. (2008) Increases in intracellular calcium triggered by channelrhodopsin-2 potentiate the response of metabotropic glutamate receptor mGluR7. *J Biol Chem* 283(36):24300–24307.
42. Inagaki N, Honma S, Ono D, Tanahashi Y, Honma K (2007) Separate oscillating cell groups in mouse suprachiasmatic nucleus couple photoperiodically to the onset and end of daily activity. *Proc Natl Acad Sci USA* 104(18):7664–7669.
43. Myung J, et al. (2015) GABA-mediated repulsive coupling between circadian clock neurons in the SCN encodes seasonal time. *Proc Natl Acad Sci USA* 112:E3920–E3929.
44. Kunz H, Achermann P (2003) Simulation of circadian rhythm generation in the suprachiasmatic nucleus with locally coupled self-sustained oscillators. *J Theor Biol* 224(1):63–78.
45. Ueda HR, Hirose K, Iino M (2002) Intercellular coupling mechanism for synchronized and noise-resistant circadian oscillators. *J Theor Biol* 216(4):501–512.
46. Ermentrout GB, Terman DH (2010) *Mathematical Foundations of Neuroscience*, Interdisciplinary Applied Mathematics (Springer Science+Business Media, New York), Vol 35.
47. Bagheri N, Taylor SR, Meeker K, Petzold LR, Doyle FJ, 3rd (2008) Synchrony and entrainment properties of robust circadian oscillators. *J R Soc Interface* 5(Suppl 1): S17–S28.